Nonlocal Damping of Helicon Waves*

J. R. HOUCK† AND R. BOWERS‡
Laboratory of Atomic and Solid State Physics, Cornell University, Ithaca, New York

(Received 14 August 1967)

The nonlocal damping of helicon waves propagating in the simple metals is discussed. An approximate dispersion relation is presented which includes the effects of both normal collision damping and nonlocal damping. Two types of experiments designed to measure the damping in sodium and potassium are described. The first type involves measurements of the standing-wave resonances in thin-plate sodium samples. This technique is useful in the regime $ql<5$, where q is the helicon wave vector and l is the carrier mean free path. The second type involves transmission experiments using both sodium and potassium. These experiments span the range $4\lesssim ql\lesssim 30$. The experimental results are in close agreement with the theoretical predictions based on the free-electron model.

I. INTRODUCTION

THE nonlocal damping of plasma waves was first studied by Landau in 1946[1]; since then, the discussion has been extended to other types of plasma excitations.[2] We wish to report the observation of the nonlocal damping of helicon waves in the alkali metals at liquid-helium temperatures. Experiment and theory are in close agreement and provide another example of the use of solid-state plasmas to investigate phenomena more commonly associated with gaseous plasmas.

In this paper the term nonlocal damping refers to the collisionless attenuation due to the coherent interaction between the wave and those carriers which are drifting along the external magnetic field B_0 at velocities near the phase velocity of the helicon wave. Since the helicon phase velocity is much less than the Fermi velocity ($V_{\text{phase}}/V_{\text{Fermi}}\approx 10^{-5}$), only electrons very near the belly of the Fermi surface contribute to the damping. This is in contrast to Doppler shifted cyclotron resonance (DSCR) which involves electrons whose velocity component along the external magnetic field is near the Fermi velocity.[3] Furthermore, DSCR occurs for helicon propagation in any direction relative to B_0, while the type of nonlocal damping discussed here exists only if the angle between the helicon wave vector and B_0 is nonzero. An extensive bibliography of DSCR as well as other topics related to helicon propagation is given by Bowers and Steele.[4] The present discussion is limited to the case of a spherical Fermi surface. The theory of the damping for a nonspherical Fermi surface has been developed by Walpole and McWhorter.[5]

* Submitted in partial fulfillment of the Ph.D. requirements, Cornell University, Ithaca, N.Y. This work was supported by the Atomic Energy Commission Contract No. AT(30-1)-2150, NYO-2150-33, and the Advanced Research Projects Agency.

† National Science Foundation predoctoral fellow during much of this work; present address: Center for Radiophysics and Space Research, Cornell University, Ithaca, N.Y.

‡ On leave: Office of Science and Technology, Washington, D.C.

[1] L. Landau, J. Phys. **10**, 25 (1946).

[2] See, for example, D. Pines and J. R. Schrieffer, Phys. Rev. **124**, 1387 (1961).

[3] M. T. Taylor, Phys. Rev. **137**, A1145 (1965).

[4] R. Bowers and M. C. Steele, Proc. IEEE **52**, 1105 (1964).

[5] J. N. Walpole and A. L. McWhorter, Phys. Rev. **158**, 708 (1967).

II. THEORY

A semiquantitative model of the trapping of particles by longitudinal plasma waves has been given by Jackson.[6] His discussion can be easily adapted to the case of helicon propagation in a collisionless plasma. This model will be briefly outlined before the more formal treatment is discussed. The fields of a helicon wave propagating along the external magnetic field B_0 are essentially transverse to the direction of propagation. Therefore, particles moving along B_0 do not experience forces in the direction of their motion. However, if the helicon is propagating at some nonzero angle ϕ to B_0 there are components of the helicon fields along B_0 and hence in the direction of the particle motion. These fields give rise to forces which are able to trap particles moving at a velocity near the phase velocity of the wave. As pointed out by Buchsbaum and Platzman,[7] the most important forces arise from the helicon's magnetic field. The component of the helicon's magnetic field along B_0 alternately adds to and subtracts from the external field, hence the local magnetic field in the material oscillates in magnitude as one moves along a line parallel to B_0 (such a line is, in fact, nearly a guiding center for a charged particle in the material). Therefore, as the particles drift along the field, they experience regions of alternately increasing and decreasing magnetic field. These "ridges" in the magnetic field act as magnetic mirrors which tend to restrict the particle motion along the field. If a particle becomes trapped by the wave, in general there is an exchange of energy between the wave and the particle. Particles which are initially moving along B_0 at a velocity less than $V_p/\cos\phi$ (V_p is the helicon phase velocity) absorb energy from the wave. More rapidly moving particles deliver energy to the wave. Under conditions of thermal equilibrium, there are more particles moving slower than the wave, hence there is a net transfer of energy to the particle system resulting in the attenuation of the wave.

[6] J. D. Jackson, J. Nucl. Energy Pt. C **1**, 171 (1960).

[7] S. J. Buchsbaum and P. M. Platzman, Phys. Rev. **154**, 395 (1967).

The magnitude of the damping can be found by integrating the energy transfer as a function of particle velocity over the distribution function for the particles.

This simple theory, which does not include ordinary collisions, is discussed from a more formal point of view by Kaner and Skobov.[8] Their result is essentially the same as that obtained from the simple kinetic model. If normal collisions are included, the theoretical analysis becomes complicated because normal collisions destroy the coherence between the particles and the wave. The reduced coherence results in a decrease in the nonlocal damping.

The nonlocal attenuation of helicon waves, including the effects of collisions, can be treated formally by deriving the helicon dispersion relation using the nonlocal conductivity tensor.[9] One finds the following approximate dispersion relation[7,10]:

$$\omega=\frac{RB_0}{\mu_0}q^2\cos\phi\left[1+i\left(\frac{1}{\omega_c\tau\cos\phi}+\frac{3\pi}{16}\frac{qV_F}{\omega_c}f(q_zl)\sin^2\phi\right)\right]. \tag{1}$$

R is the Hall constant, q the helicon wave vector, ω_c the cyclotron frequency, τ the reciprocal of the collision frequency, and V_F the Fermi velocity. The second term in the imaginary part of Eq. (1) represents the nonlocal damping and is zero for propagation along B_0. The function $f(q_zl)$ reflects the reduction in the nonlocal damping due to collisions. For $q_zl=0$, f is equal to zero; in the absence of collisions $f=1$. The functional form of f is[11]

$$f(x)=(16/3\pi)\{-(2x)^{-1}+\tfrac{3}{16}F(x)+[x/6H(x)][G(x)-1]^2\},$$

where

$$F(x)=2\tan^{-1}x-(x-\tan^{-1}x)[(4/x^2)+(2/x^4)]+(2/3x),$$

$$G(x)=1+(3/2x^2)-(3/2x)[1+(1/x^2)]\tan^{-1}x,$$

$$H(x)=1-(1/x)\tan^{-1}x.$$

It is to be emphasized that Eq. (1) is only an approximate dispersion relation. A careful discussion of the limits of its validity is given in Ref. 10.

In the next sections the experiments designed to check Eq. (1) are described. Two different experimental techniques were used. The first involved the observation of the standing-wave modes of a thin plate; in order to achieve wavelengths which are smaller than the electron mean free path ($ql>1$), one excites harmonics of the fundamental resonance. The second technique involved the transmission of helicon waves through a thin plate; small wavelengths are achieved in this case by increasing the frequency of the impressed signal. Preliminary experiments have previously been described elsewhere.[10,12–14]

III. STANDING-WAVE EXPERIMENTS

Standing-wave helicon resonances can be excited in samples of many geometries.[15] These resonances depend on the dimensions of the samples, and roughly correspond to a half-integer number of helicon wavelengths "fitting" the various dimensions of the sample. By measuring the frequency and quality factors of these resonances as a function of magnetic field, information can be obtained about the Hall coefficient and resistivity of the material. Although these dimensional resonances are easy to observe in many geometries, an exact theory of the mode structure is well established only for the case of the *infinite* thin plate. However, in practice, the resonances of a *finite* thin plate whose thickness is less than about 10% of its width are well described by the theory for the infinite thin plate.

The theoretical analysis of the mode structure of an infinite thin plate was first discussed by Chambers and Jones.[16] Their theory predicts the following relations between the amplitude h and quality factor Q of the resonances:

$$Q=\tfrac{1}{2}(1+u^2)^{1/2},\qquad u=RB_0/\rho,\qquad h\propto u,$$

where R and ρ are the Hall coefficient and resistivity of the bulk material.

Using the same approximations Penz[17] has extended the Chambers and Jones theory to the case of an arbitrary resistivity tensor. In the limit of high conductivity ($\rho_{12}\gg\rho_{11}$) he finds

$$h\propto Q\propto[(\rho_{12}\rho_{21})^{1/2}/(\rho_{11}+\rho_{22})],$$

where q is parallel to the (3) axis. This reduces to

$$h^{-1}\propto\{(\omega_c\tau\cos\phi)^{-1}+(3\pi/16)(qV_F/\omega_c)f(q_zl)\sin^2\phi\}, \tag{2}$$

which is exactly the ratio between the real and imaginary parts of the dispersion relation, Eq. (1). Thus the nonlocal part of the dispersion relation can be studied by measuring the resonant amplitude as a function of angle ϕ. By observing the high-order resonances ($n>1$), the dependence upon qv_F/ω_c and q

[8] E. A. Kaner and V. G. Skobov, Zh. Eksperim. i Teor. Fiz. **45**, 610 (1963) [English transl.: Soviet Phys.—JETP **18**, 419 (1964)].
[9] M. H. Cohen, M. J. Harrison, and A. W. Harrison, Phys. Rev. **17**, 937 (1960).
[10] J. R. Houck, Ph.D. thesis, Cornell University, 1967 (unpublished).
[11] The notation used here is similar to that of Platzman and Buchsbaum.
[12] C. C. Grimes, Bull. Am. Phys. Soc. **11**, 570 (1965).
[13] J. R. Houck and R. Bowers, Bull. Am. Phys. Soc. **11**, 256 (1965); Atomic Energy Commission Report No. NYO-2150-15 (unpublished).
[14] C. C. Grimes and A. Libchaber Bull. Am. Phys. Soc. **12**, 771 (1967).
[15] F. E. Rose, Ph.D. thesis, Cornell University, 1965 (unpublished).
[16] R. G. Chambers and B. K. Jones, Proc. Roy. Soc. (London) **A270**, 417 (1962).
[17] P. A. Penz, Ph.D. thesis 1967 (unpublished and Materials Science Center, Cornell University Report No. 440, 1966 (unpublished).

can be checked. If a particular resonance is observed for a variety of magnetic fields, the dependence upon qv_F/ω_c can be separated from the q dependence. The amplitude dependence of the resonances is discussed in detail in a later section.

A. Experimental Technique

The standing-wave resonances were observed using the conventional cross coil experiment in which the thin-plate sample is surrounded by two orthogonal coils. The resonances are excited by a constant-current variable-frequency signal applied to one coil and appear as a voltage induced in the second coil.[18] The conventional arrangement was modified to allow variation of the angle between the sample normal and B_0.

The signal generated in the pickup coil was typically 100 μV. It was amplified and the detected amplitude was plotted as a function of excitation frequency on an X–Y recorder. Both modulus and phase-sensitive detection were used and yielded essentially the same results.

All samples used in the standing-wave experiments were pressed polycrystalline sodium plates. They were 10 mm on a side and ranged between $\frac{1}{2}$ and 2 mm in thickness. (Disk-shaped samples 10 mm in diameter were also used.) The samples were prepared by pressing

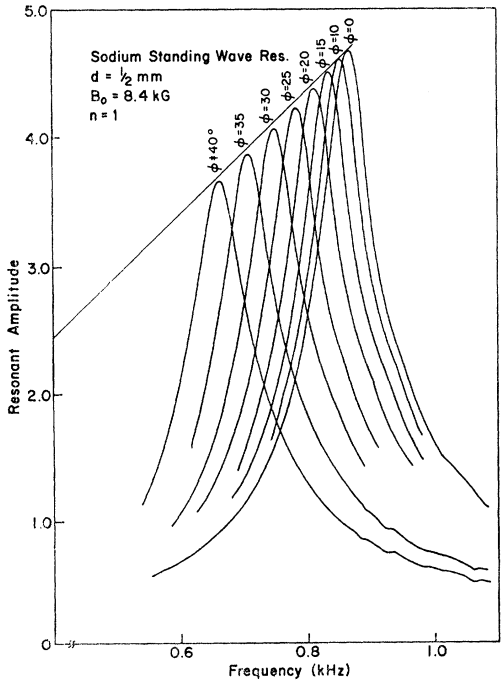

FIG. 1. Standing-wave helicon resonances in the local limit as a function of ϕ. The local theory predicts a linear relation between the resonant amplitude and resonant frequency. The straight line is a line through the origin.

[18] F. E. Rose, M. T. Taylor, and R. Bowers, Phys. Rev. **127**, 1122 (1962).

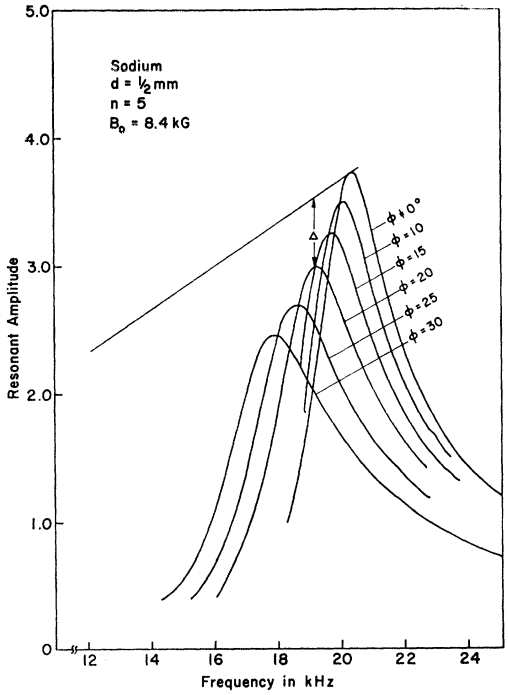

FIG. 2. Standing-wave helicon resonances under conditions of nonlocal conductivity. The straight line passes through the origin. At $\phi \neq 0$ the resonant amplitude is less than that predicted by the local theory. This extra decrease in amplitude is due to nonlocal damping.

a block of oil covered sodium between two stainless steel plates using "Saran Wrap" as a buffer between the stainless steel and the sodium. After pressing, the samples were cut to size with a razor blade.

The sodium had residual resistance ratios between room temperature and 4.2°K of 5000 to 8000. It is helpful to remember that the $\omega_c\tau/B_0 \approx 1$ for the purest material if B_0 is measured in kG. The mean free path l is approximately 0.1 mm.

B. Experimental Results

Figure 1 shows the dependence on ϕ of the $n=1$ resonance (one-half wavelength equals the sample thickness) observed for a $\frac{1}{2}\times 10\times 10$ mm sodium plate; under these experimental conditions $ql<1$, so that nonlocal effects can be neglected. Figure 2 shows similar data for the $n=5$ resonance. For these resonances $ql \simeq 4.5$ and nonlocal effects are important.

For any angle ϕ the helicon wave vector is essentially perpendicular to the sample face. This is a consequence of the symmetry imposed by the boundaries of the sample. Therefore,

$$q = n\pi/d,$$

where d is the sample thickness. n is an integer and is equal to the number of half-wavelengths spanning d. The corresponding resonant frequencies are given by

$$\omega_R(n) = (RB_0/\mu_0)\,(n\pi/d)^2 \cos\phi.$$

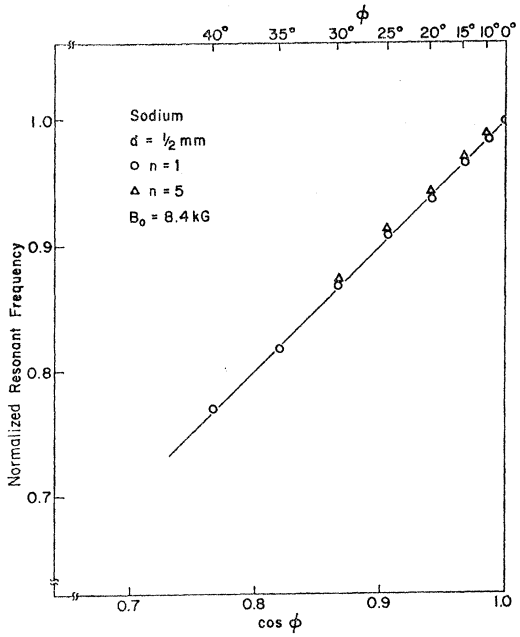

FIG. 3. Resonant frequency as a function of $\cos\phi$. According to the local theory, the resonant frequency is proportional to $\cos\phi$. The nonlocal correction to the resonant frequency is small and varies slowly with ϕ. The resonant frequencies for two resonances shown very nearly fit the expected $\cos\phi$ dependence.

Figure 3 shows a plot of ω_R as a function of ϕ for two resonances, the $n=1$ resonance of Fig. 1 and the $n=5$ resonance of Fig. 2. It is evident that the resonant frequencies have an accurate $\cos\phi$ dependence in both cases. The resonant peaks of the $n=5$ resonance have a $\cos\phi$ dependence, even though nonlocal conditions clearly exist ($qv_F/\omega_c=0.2$, $ql=4.5$). This is in agreement with theory; the nonlocal corrections to the real part of the dispersion relation are small for $qv_F/\omega_c<0.5$. The first nonzero correction to the real part of the dispersion relation varies as $(qv_F/\omega_c)^2$ and is only weakly dependent on ϕ.[10] (For $qv_F/\omega_c=0.2$ this correction is of the order of 0.8%.)

If there are no nonlocal corrections to the dispersion relation, Eq. (2) predicts

$$h_L \propto u\cos\phi = \omega_c\tau\cos\phi.$$

Notice also that there is a linear relation between $\omega_R(n)$ and the resonant amplitude only if nonlocal damping is absent.

$$h_L \propto \omega_c\tau\cos\phi \propto \omega_R.$$

In Fig. 1 it is clear that this linear relationship is obeyed, indicating that the nonlocal correction to the amplitude is small for the $n=1$ resonance.

The amplitudes of the resonances in Fig. 2 are seen to deviate markedly from the straight line, indicating that there is more damping at $\phi>0$ than would be predicted by a simple extrapolation of the collision damping observed at $\phi=0$. This additional attenuation is due to nonlocal damping.

A direct measure of the nonlocal damping is given by Δ which is the difference between the peak height at angle ϕ and the height of the straight line (see Fig. 2). Equation (2) gives the following relation between Δ and $f(q_zl)$:

$$\Delta/h_L \mid_\phi = (3\pi/16)\,qlf(q_zl)\sin^2\phi\cos\phi,$$

where Δ/h_L is evaluated at angle ϕ. The angular dependence of Δ/h_L for the resonances of Fig. 2 is shown in Fig. 4. If $f(q_zl)$ were independent of ϕ, Δ/h_L would depend linearly upon $\sin^2\phi\cos\phi$, the slope being determined by ql. However, as ϕ increases, q_zl and f decrease. For the data of Fig. 2 the theory predicts that $f(4.5\cos\phi)$ will decrease by approximately 8% between $\phi=0$ and $\phi=30°$. The experimental points agree well with the solid curve which is the theoretical curve for $ql=4.5$. The free-electron parameters of sodium were used for the data reduction[3]

$$K_F = 0.923\times10^{10}\ \mathrm{m}^{-1},$$
$$|R| = 23.6\times10^{-11}\mathrm{C/m}^3;$$

hence,

$$qv_F/\omega_c \simeq 1.11\nu^{1/2}(10/B)^{3/2} \quad \text{for} \quad qv_F/\omega_c<0.5$$

(where ν is measured in MHz and B_0 is in kG). ql is given by

$$ql = (qv_F/\omega_c)\omega_c\tau = (qv_F/\omega_c)\,u,$$

where u is determined from the Q of the resonance.

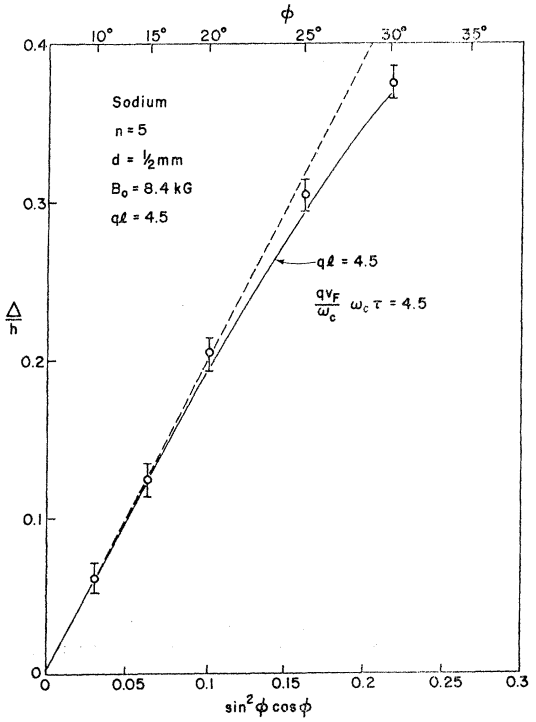

FIG. 4. The deviation of the resonant amplitude from the prediction of the simple theory. The data plotted are from the curves shown in Fig. 2. The theoretical curve assumes $ql=4.5$.

In all cases the Q used to calculate ql for a particular resonance is the quality factor of that resonance at $\phi=0$.

As shown above, it is possible to obtain an experimental value for $qlf(q_zl)$ from plots of the type shown in Fig. 2. Thus one can compare the experimentally measured nonlocal damping with ql determined from the local characteristics $[Q(\phi=0)]$ of the resonance and the constants of the material (K_F and $|R|$). Figure 5 shows a plot of $qlf(q_zl)$ as a function of q_zl for the standing-wave experiments. The solid curve is the prediction of the detailed theory which includes the effects of ordinary collisions. The dashed line is the prediction of the simple theory. The results closely agree with the predictions of the free-electron theory for $ql<5$. However, the method cannot be used with confidence for larger ql because the high-order resonances required to reach $ql>5$ begin to overlap causing complicated shifts of the zero line. Of course, thinner samples could be used in an attempt to study the large ql region using the low-order resonances ($n=1$, 3, 5) which are well separated. However, under these circumstances, the electron mean free path is of the order of the sample thickness and complications due to size effects become important. It is possible to circumvent this problem and study the high ql regime by making use of propagation experiments. The results of these experiments are described in the next section.

IV. TRANSMISSION EXPERIMENTS

As pointed out in the last section, the standing-wave resonance method is not useful when $ql>5$ because of the complicated overlapping of neighboring resonances. In order to investigate the characteristics of the nonlocal damping at larger ql, a series of transmission experiments was undertaken. The magnitude of q is increased by raising the frequency of the impressed signal. In the present experiment, the *amplitude* of the transmitted signal is measured as the angle between q and B_0 is varied. In this respect, these experiments differ from previous measurements which were concerned with the frequency-field relation of changes in the transmitted signal.

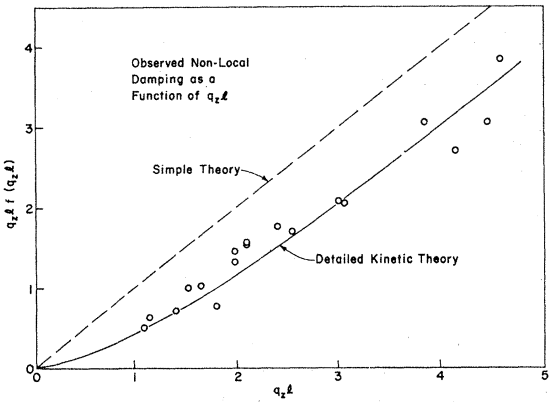

FIG. 5. Nonlocal damping as a function of q_zl. The coefficient of the $\sin^3\phi$ term in the damping is plotted as a function of q_zl. The straight line is the prediction of the Kaner and Skobov theory. The curve is the result of the more detailed kinetic theory. The experimental points represent the results of measurements on different sodium samples.

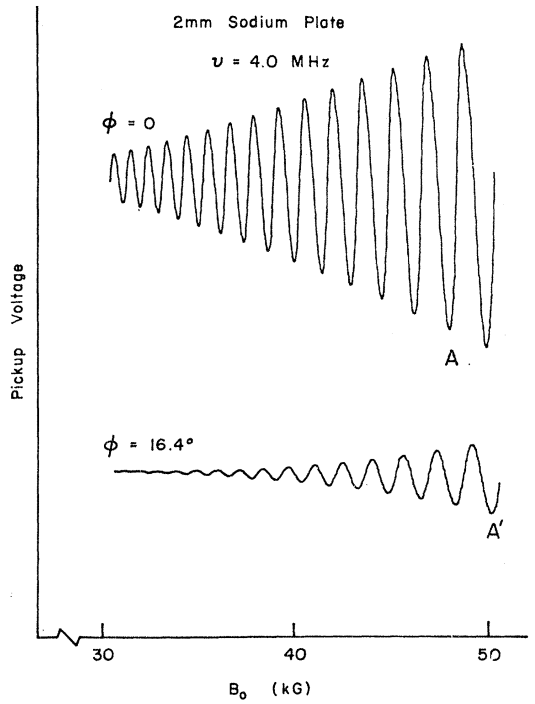

FIG. 6. The transmission fringe pattern. The fringe pattern results from the interference between the signal which "leaks" around the sample and the signal due to the transmitted helicon wave. The upper curve corresponds to $\phi=0$. The lower curve, which has been displaced for clarity, corresponds to $\phi=16.4°$. The reduced amplitude of the lower curve is due to nonlocal damping.

A. Experimental Technique

In the transmission experiments, the excitation and pick coils are on either side of the thin-plate sample and are carefully shielded from one another to reduce direct coupling (leakage).[19] Provision was made to adjust the angle between the sample normal and B_0. The total voltage appearing across the receiver coil is the sum of contributions from the helicon signal and the leakage signal. The interference of these signals gives rise to a fringe pattern. Figure 6 shows a photocopy of the fringe pattern observed for a $2\times12\times14$ mm sodium plate at 4.0 MHz. The upper and lower curves correspond to $\phi=0$ and $\phi=16.4°$, respectively. The curves have been displaced vertically for clarity.

The thickness of the sample d, excitation frequency ν, and magnetic field B_0 are chosen such that the helicon signal is strongly attenuated by a single traversal of the

[19] C. C. Grimes and S. J. Buchsbaum, Phys. Rev. Letters **12**, 357 (1964).

sample. Therefore the contribution from multiple reflections of the helicon wave inside the sample can be ignored compared to the direct transmission.

The contribution due to the transmitted helicon wave is of the form

$$A_2 = a_2 \sin(\omega t + \theta).$$

Both the amplitude and phase of this component depend upon the sample thickness and the properties of the helicon wave.

The direct pickup or leakage signal is independent of changes in B_0 and ϕ and is of the form

$$A_1 = a_1 \sin \omega t.$$

The detection of the sum of these voltages gives

$$A_{\text{rms}} \propto (a_1 + a_2 \cos\theta)\{1 + \tfrac{1}{2}[a_2/(a_1 + a_2\cos\theta)]^2 \cdots\}.$$

If $a_1 \gtrsim 10 a_2$, then, to a good approximation, the amplitude of the envelope of the detected signal is proportional to the amplitude of the transmitted helicon signal a_2. The phase of the modulation is determined by the phase delay introduced by the helicon.

Assuming a plane wave normally incident on an infinite thin lossy dielectric slab, the transmitted amplitude a_2 is given by

$$a_2 = a_0 T^2 \exp(-q_i d).$$

q_i is the imaginary part of q, d is the thickness of the slab, and T is the transmission coefficient at the two surfaces. From Eq. (1) this becomes

$$a_2 = a_0 T^2 \exp\{-\tfrac{1}{2}(d/\lambda)[(1/\cos^{3/2}\phi) \times (\omega_c\tau)^{-1} + (qv_F/\omega_c) f(q_z l)(\sin^2\phi/\cos\phi)]\}. \quad (3)$$

For a refractive index $\eta \gg 1$, one finds $T \propto \eta^{-1/2}$. For the helicon case at constant frequency this reduces to

$$T^2 \propto \cos^{1/2}\phi.$$

However, the angular dependence of the transmitted amplitude is dominated by the angular dependence of q_i in the exponent. The angular dependence of T^2 seldom effects the value of $q_i d$ derived from the observed amplitude by more than 1%.

B. Data Analysis

Almost all of the pertinent information can be obtained from two curves of the type shown in Fig. 6. Only one additional measurement, an independent determination of the collision damping, is necessary.

The analysis of the data can be divided into two steps: the determination of the sample thickness and angle ϕ from the over-all aspects of the fringe pattern and the analysis of the angle and field dependence of the damping. These two parts are discussed separately.

1. Over-All Aspects of the Fringe Pattern

Consider first the curve corresponding to $\phi = 0$. The spacing between the various peaks is not constant but is in fact a function of the number of helicon wavelengths spanning the sample. Successive peaks in the direction of decreasing field correspond to $d/\lambda = N$ increasing by 1. The fields of two adjacent peaks are related by

$$(N+1)/N = B_N/B_{N+1}.$$

In this way one can directly determine d/λ, the quantity entering into Eq. (3). Thus, no mechanical measurement of the sample thickness is necessary.

Returning to Fig. 6, notice also that the peaks shift in position as the sample is rotated. In fact, for the data shown, the shift in the phase was more than 360°. As ϕ was increased from zero, peak A shifted uniformly to A'. This shift in position is proportional to cos ϕ and allows one to accurately determine ϕ. The value of ϕ derived in this way typically agrees with the mechanically determined value to within 0.3°.

2. The Dependence of the Damping on Angle and Magnetic Field

From the ratio of the envelopes of the curves of the type shown in Fig. 6, the increase in damping at $\phi \neq 0$ can be determined. If R is the ratio of the envelope amplitudes at some field B_0, then

$$R = (T_0/T)^2 \exp[-\tfrac{1}{2}(d/\lambda)\{(1 - 1/\cos^{3/2}\phi) \times (\omega_c\tau)^{-1} + (qv_F/\omega_c) f(q_z l)(\sin^2\phi)/\cos\phi\}], \quad (4)$$

where q and d/λ on the right side refer to their respective values at $\phi = 0$. The dependence of Eq. (4) on ϕ, B_0, q, and τ is rather involved and will be discussed in some detail.

(*a*) *Angular Dependence.* A small angle expansion of the angular-dependent functions in Eq. (4) yields

$$1 - (1/\cos^{3/2}\phi) = \tfrac{3}{4}\phi^2 + \tfrac{15}{32}\phi^4 \cdots,$$

$$\tfrac{3}{4}(\sin^2\phi/\cos\phi)\phi = \tfrac{3}{4}\phi^2 + \tfrac{1}{8}\phi^4 \cdots.$$

The leading term in both expansions involves ϕ^2, and the coefficients of ϕ^4 terms are of similar magnitude. Even at $\phi = 20°$, the functions differ by only 2%. For this reason it is nearly impossible to separate the local and nonlocal terms of Eq. (4) on the basis of their angular dependence. However, the collision term can be determined independently by using a sufficiently low excitation frequency (and $\phi = 0$). At reduced frequency and the highest magnetic fields, clearly defined standing-wave resonances were observed. From these resonances Q and hence $\omega_c\tau$ can be determined. In this way the attenuation due to collision processes can be measured without the necessity of making an absolute determination of the transmitted power. The value of $\omega_c\tau$ obtained is used in the calculation of ql as described earlier.

Figure 7 shows a plot of log R as a function of $\sin^2\phi/\cos\phi$. The measurements were made at 2.0 MHz with $B_0 = 36.7$ kG. It is evident that the increase in

damping due to rotation agrees well with the angular dependence predicted by the theory.

(*b*) *Magnetic Field Dependence.* The magnetic field enters the nonlocal part of Eq. (4) through ω_c and q in the form

$$(q^2/\omega_c)f(q_z l).$$

For modest variations in B and for $ql \gtrsim 10$, the variation of $f(q_z l)$ can be ignored. Using the local dispersion relation and assuming constant frequency one has

$$q^2/\omega_c \propto 1/B^2,$$

while the damping due to collision varies as

$$q/\omega_c \propto 1/B^{3/2}.$$

Thus for moderate variations in B (30–50kG) the local and nonlocal terms scale by roughly the same amount.

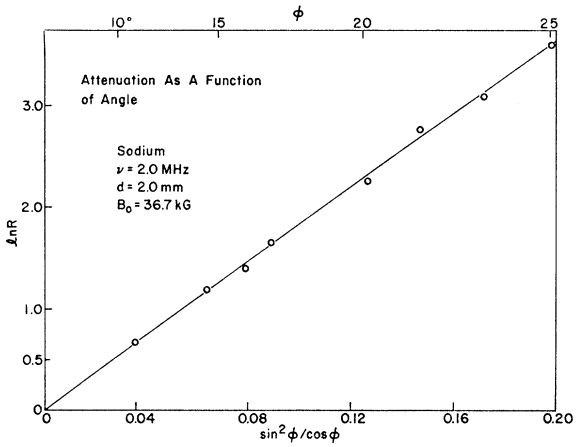

FIG. 7. Relative amplitude of transmitted signal as a function of angle. The log of the ratio of the fringe envelopes at $B_0 = 36.7$kG is plotted as a function of $\sin^2\phi/\cos\phi$. The nonlocal theory predicts a nearly linear relationship for $q_z l \gg 1$.

The important point to remember is that while both the angular and field dependence of the two terms are similar, the increase in attenuation upon rotation is roughly 10 times too large to be explained solely on the basis of collision damping. A plot of log R as a function of $1/B^2$ is shown in Fig. 8. The points represent measurements made at various frequencies using a 2-mm sodium plate. The points very nearly fit a straight line through the origin, as predicted by the free-electron theory.

From the slope of curves similar to those in Fig. 8, an experimental value for the exponent in Eq. (4) can be determined. The effects of collision damping are subtracted out; so that the remainder is a measure of the nonlocal damping. The ratio of the observed damping divided by the damping predicted by the simple theory $[f(q_z l) = 1]$ is shown as a function of $q_z l$ in Fig. 9. The open circles are the results of transmission experiments using sodium. The solid circles are the standing-wave results of Fig. 5. The triangles represent the results of measurements made using potassium samples. The

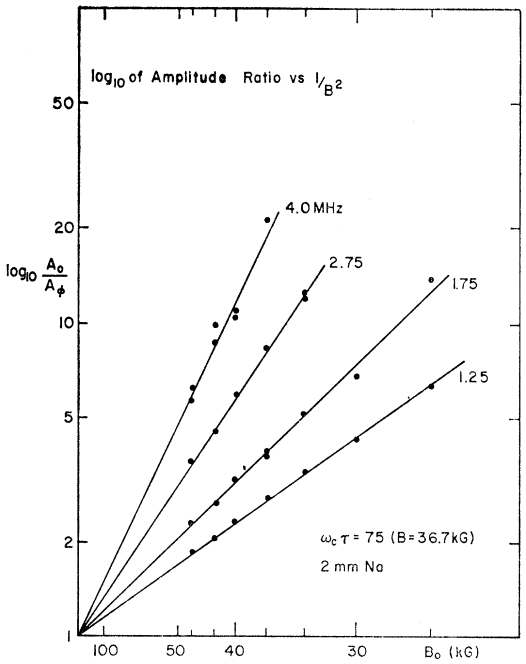

FIG. 8. Nonlocal damping as a function of magnetic field. The log of the ratio of the fringe envelopes is plotted as a function of $1/B^2$ for $\phi = 16.4°$. The free-electron theory predicts a linear dependence.

value of qv_F/ω_c for potassium differs from that of sodium by nearly a factor of 2 under the same experimental conditions. The free-electron parameters of potassium are[3]

$$K_F \text{ (potassium)} = 0.746\times 10^{10}\text{m}^{-1},$$

$$R \text{ (potassium)} = -44.5\times 10^{-11}\text{m}^3/\text{C}.$$

Therefore

$$qv_F/\omega_c \text{ (potassium)} = \nu^{1/2}(10/B_0)^{3/2}0.654,$$

where ν is the excitation frequency in MHz and B_0 is

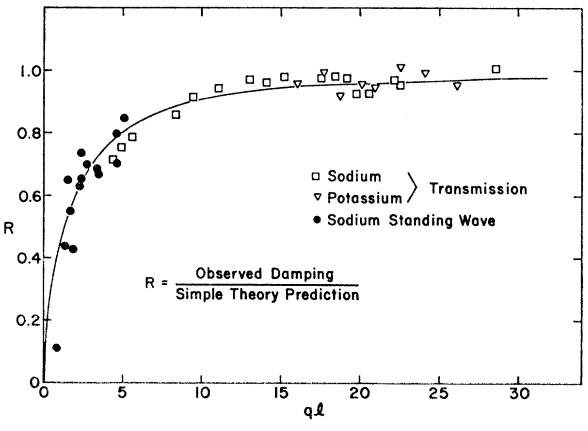

FIG. 9. Collected results of the nonlocal damping studies. The observed nonlocal damping is plotted as a function of ql. The curve is the prediction of the free-electron theory.

measured in kG. (The parameters for sodium were given in Sec. III.)

The transmission measurements were made at frequencies between 1.0 and 8.0 MHz at fields between 15 and 50 kG. In the standing-wave experiments the frequency ranged between 0.5 and 50 kHz while the field was varied between 4.3 and 16.7 kG. Thus Fig. 9 shows good agreement between theory and experiment over a wide range of experimental conditions.[20]

V. CONCLUSIONS

In summary, experimental results obtained with sodium and potassium closely agree with the predictions of the free-electron theory over a wide range of experimental conditions. The form of the theoretical correction to the nonlocal damping due to collision processes agree well with experiment.

[20] The nonlocal damping of helicon waves has been measured using pulse techniques. The results of the pulsed experiments are also in close agreement with the free-electron theory.

The high degree of agreement is particularly gratifying since the experiment gives a check on a rather involved transport-theory calculation in which there are no adjustable parameters. The Fermi momentum is the only parameter which cannot be measured directly by the experiments. However, the free-electron value which we have used agrees with the value measured by Shoenberg and Stiles[21] using the de Haas–van Alphen effect within 0.5%.[1]

ACKNOWLEDGMENTS

We wish to thank M. Lampert and R. G. Chambers for pointing out that corrections to the simple nonlocal theory are necessary if normal collisions are present. The authors had many helpful discussions with B. W. Maxfield during the course of this work. We also wish to acknowledge the valuable help of J. C. Garland in the preparation of the manuscript.

[21] D. Shoenberg and P. J. Stiles, Proc. Roy. Soc. (London) **A281**, 62 (1964).

PHYSICAL REVIEW VOLUME 166, NUMBER 2 10 FEBRUARY 1968

Flux Quantization in a One-Dimensional Model*

MICHAEL SCHICK†
Department of Physics, Stanford University, Stanford, California

(Received 11 September 1967)

A one-dimensional model of interacting electrons is studied to determine whether such a system, in thermal equilibrium, can exhibit flux quantization. The free energy and current of the system are calculated and shown to be periodic functions of the flux enclosed in a ring-shaped sample with period hc/e. The Maxwell equations provide a second relation between the current and flux. It is found that at finite temperatures, the equations for the current I and the flux Φ_B have only the trivial solution $I=\Phi_B=0$ in the limit of macroscopic systems. Therefore, there is no flux quantization. The free energy is calculated by a generalization of the method of Tomonaga. This method describes the Fermi system in terms of an equivalent set of bosons which represent the collective modes of the Fermi gas. The major results of the generalization are the appearance of trilinear terms in the equivalent boson Hamiltonian and effects of a vector potential.

1. INTRODUCTION

SINCE the suggestion by Little[1] that properly synthesized long organic polymers might be superconducting at room temperatures, there has been renewed interest in the properties of one-dimensional electron systems. Recently, Hohenberg[2] has rigorously proved that a one-dimensional system cannot exhibit off-diagonal long-range order (ODLRO),[3] a property characteristic of superconductors in three dimensions. However, the absence of ODLRO does not imply the absence of other properties characteristic of superconductivity such as flux quantization and persistent currents as discussed in Sec. 4. The possibility of the existence of flux quantization and persistent currents in nonequilibrium situations has been investigated by Little,[4] and Ambegaokar and Langer.[5]

It is the purpose of this paper to examine a one-dimensional model of interacting electrons to determine whether the system can exhibit flux quantization in equilibrium.[6] The analysis is directed to the calculation of the free energy of the system (Sec. 3), which is shown

* Supported by the U.S. Office of Naval Research under Contract No. NONR-225(75).

† Present address: Department of Physics, Western Reserve University, Cleveland, Ohio.

[1] W. A. Little, Phys. Rev. **134**, A1416 (1964).

[2] P. C. Hohenberg, Phys. Rev. **158**, 383 (1967).

[3] C. N. Yang, Rev. Mod. Phys. **34**, 694 (1962).

[4] W. A. Little, Phys. Rev. **156**, 396 (1967).

[5] J. S. Langer and V. Ambegaokar, Phys. Rev. (to be published).

[6] Whereas "one-dimensional" means for Refs. 4 and 5 that the transverse dimensions of the system are small compared to the temperature-dependent correlation length and penetration depth, for this paper it will be taken to mean that those states which correspond to transverse electron motion contribute negligibly to the partition function. In general, this imposes the more severe condition that the transverse extension be smaller or of the order of the Fermi wavelength.